Biomaterials 35 (2014) 1552–1561

Contents lists available at ScienceDirect

Biomaterials

journal homepage: www.elsevier.com/locate/biomaterials

Molecular mechanisms of anticancer action and cell selectivity of short α-helical peptides

Cuixia Chen [a], Jing Hu [a], Ping Zeng [a], Fang Pan [b], Mohammed Yaseen [b], Hai Xu [a,*], Jian R. Lu [b,*]

[a] Centre for Bioengineering and Biotechnology, China University of Petroleum (East China), 66 Changjiang West Road, Qingdao 266580, China
[b] Biological Physics Laboratory, School of Physics and Astronomy, University of Manchester, Schuster Building, Manchester M13 9PL, UK

ARTICLE INFO

Article history:
Received 6 September 2013
Accepted 31 October 2013
Available online 15 November 2013

Keywords:
Antimicrobial peptide
Anticancer activity
Cell selectivity
Membrane permeabilization
Cell apoptosis
Xenograft model

ABSTRACT

Development of functional biomaterials and drugs with good biocompatibility towards host cells but with high potency against cancer cells is a challenging endeavor. By drawing upon the advantageous features of natural antimicrobial peptides and α-helical proteins, we have designed a new class of short α-helical peptides $G(IIKK)_nI\text{-}NH_2$ ($n = 1–4$) with different potency and high selectivity against cancer cells. We show that the peptides with $n = 3$ and 4 kill cancer cells effectively whilst remaining benign to the host cells at their working concentrations, through mechanistic processes similar to their bactericidal effects. The high cell selectivity could stem from their preferential binding to the outer cell membranes containing negative charges and high fluidity. In addition to rapid membrane-permeabilizing capacities, the peptides can also induce the programmed cell death of cancer cells via both mitochondrial pathway and death receptor pathway, without inducing non-specific immunogenic responses. Importantly, these peptides can also inhibit tumor growth in a mouse xenograft model without eliciting side effects. Whilst this study reveals the clinical potential of these peptides as potent drugs and for other medical and healthcare applications, it also points to the significance of fundamental material research in the future development of highly selective peptide functional materials.

1. Introduction

Seeking for new drugs with high potency and low toxicity or low side effects is becoming an important endeavor of functional biomaterials research. Despite tremendous advances in treatment modalities, cancers remain a major cause of mortalities worldwide. Chemotherapy is currently one of the principal strategies for treatment, especially for those at advanced or metastatic stages [1]. However, severe side effects on normal cells and tissues and the easy acquisition of multi-drug resistances by cancer cells are often intimately associated with conventional chemotherapeutical agents. Thus, the development of new anticancer drugs with low toxicity to normal host cells and a distinct mode of action that disfavors drug resistance represent the new direction in the development of more effective anticancer materials. Progress in this area could open up new applications in healthcare and treatment strategies.

Naturally occurring antimicrobial peptides (AMPs) and their synthetic analogs have been regarded as a potential source of new antibiotics for some time. AMPs have exhibited varying antimicrobial activities against a broad spectrum of microbes and interestingly, some of them have also demonstrated toxicity to cancer cells but the extent of biocompatibility to normal mammalian cells varies [2–4]. Furthermore, because these AMPs mainly act on the target cell membranes via a non-receptor-mediated pathway, it is more difficult for cancer cells to develop resistance, compared with conventional chemotherapeutic agents [3,4]. Due to those desirable features, the investigation and exploitation of AMPs possessing cancer cell toxicity might lead to further advance in the development of better anticancer drugs. Short linear cationic AMPs that fold into amphipathic conformations when interacting with their targets represent a particularly successful structural arrangement for antibacterial peptides [5–7]. To improve their prospect in therapeutic applications and investigate structure–activity relationship, a number of analogs have been designed and synthesized to mimic the hallmarks of natural AMPs, with varying successes being reported. The primary hurdle lies in the tuning of potency over toxicity against the host cells.

* Corresponding authors.
E-mail addresses: xuh@upc.edu.cn, hai.xu@yahoo.com (H. Xu), j.lu@manchester.ac.uk (J.R. Lu).

0142-9612/$ – see front matter © 2013 Elsevier Ltd. All rights reserved.
http://dx.doi.org/10.1016/j.biomaterials.2013.10.082

In mimicry of AMPs and the structure-functional features of proteins bearing simple α-helical repeats, we have recently developed a class of short cationic peptides containing simple sequence repeats, G(IIKK)$_n$I-NH$_2$ (n = 1–4) [8]. The IIKK module promotes α-helical structuring upon contact with amphipathic membranes and as n increases, its structural propensity improves. The additional I residue at the C-terminus stabilizes the molecules and further promotes the responsiveness of the secondary structure; the C-terminal charge blocking of COO^- is delicate at triggering initial responses and subsequent selectivity tuning in response to different outer membrane surfaces. Their performance against natural AMPs and therapeutics thus requires experimental verifications.

We here show that these short synthetic peptides possess strong anticancer activities. To explore the practical relevance, we have undertaken the selectivity assessment using adult human skin dermal fibroblast cells (HDFa) under a culturing experiment approach we have developed previously using NIH 3T3 cell lines as host cells [8]. Whilst our main aim here is to investigate the mechanistic processes associated with the cell selectivity and anticancer activity of the designed peptides, the present work also examines their immunogenic responses on human lymphocytes and their therapeutic efficacies on tumor xenografts in nude mice.

2. Materials and methods

2.1. Chemical reagents and cell culture

Rink amide MBHA resin, protected amino acids, and other reagents and solvents for the peptide synthesis were purchased from GL Biochem Ltd (Shanghai, China). 3-(4, 5-dimethylthiazol-2-yl)-2, 5-diphenyltetrazolium bromide (MTT), calcein acetoxymethyl ester (Calcein-AM), 4, 6-diamidino-2-phenylindole (DAPI) and fluorescein isothiocyanate (FITC)-phalloidin were obtained from Sigma (St. Louis, Mo). 5,5′,6,6′-tetrachloro-1,1′,3,3′-tetraethylbenzimidazolcarbocyanine iodide (JC-1), anti-Cyt c monoantibody (mouse, IgG2b) and FITC-labeled goat anti-mouse secondary antibody were purchased from Beyotime Biotechnology (Jiangsu, China). Water used in all experiments was Millipore Milli-Q deionized (18.2 MΩ.cm).

HeLa (human cervical carcinoma cells) and HL60 (human promyelocytic leukemia cells) were supplied by the Cell Bank in Shanghai Institute of Cell Biology. Adult human dermal fibroblast cells (HDFa) were obtained from Invitrogen. The cancer cell lines were cultured in IMDM (Iscove's modified Dulbecco's medium) containing 10% heat-inactivated FBS (fetal bovine serum) while primary HDFa cells were cultured in M106 medium supplemented with LSGS (low serum growth supplement) and antibiotics (amoxicillin and penicillin), at 37 °C in a 5% CO_2 atmosphere.

Human lymphocytes were isolated from the whole blood cells by the standard Ficoll method. Briefly, 10 mL of blood obtained from healthy volunteers was diluted with 10 mL PBS, and then the diluted blood was carefully added to a Ficoll solution of 1.077 g/mL with the ratio of Ficoll to blood at 2:1. After centrifugation at 2000 rpm for 15 min, the ring with lymphocytes was harvested without touching the Ficoll solution. The lymphocytes were washed with PBS at least three times and then suspended in PBS for use.

Human red blood cells (h-RBCs) were isolated from the blood via centrifugation at 1000 *g*, washed three times with PBS, and then suspended to 8% (v/v) in PBS for use.

2.2. Peptide synthesis

The G(IIKK)$_n$I-NH$_2$ (n = 1–4) peptides were prepared with a commercial CEM Liberty peptide synthesizer, using standard Fmoc solid-phase peptide synthesis procedures. The synthesis was carried out from the C-terminus to the N-terminus on the Rink amide MBHA resin, thus producing C-terminally amidated peptides. More details including deprotection, coupling, and cleavage from the resin have been described previously [9–11]. Note that N-terminal FITC-labeled G(IIKK)$_3$I-NH$_2$ was synthesized also by the solid-phase chemistry and the detailed procedures were reported in our previous work [8]. After rotary evaporation, the raw peptide products were purified by cold ether precipitation at least eight times, followed by lyophilization for 2 days. The final products had high purity (>95%), as indicated by HPLC and MS analyses.

2.3. Cytotoxicity test

The *in vitro* cytotoxicity of these peptides was measured by MTT assay. Briefly, cancer or HDFa cells (~1 × 10^5 cells/mL, 100 μL) were pre-cultured in a 96-well plate. After 24 h incubation, cells were treated with 100 μL of 2-fold diluted peptide solutions (0–50 μM) and incubated for further 24 h. Then 20 μL of MTT solution (in PBS, 5 mg/mL) was added to each well and incubated for 4 h. Subsequently, the supernatants of HeLa or HDFa cells were directly removed while for HL60 cells, the culture was centrifuged at 1000 rpm for 5 min, followed by the supernatant removal. 150 μL of dimethyl sulfoxide (DMSO) was added into each well and the supernatants of the wells were transfer to a new 96 well plate and the absorbance at 570 nm was recorded using a microplate reader (M^{2}e, Molecular Devices). The wells without peptides were used for control and the wells without cells for blank of the spectrophotometer. Experiments were carried out at least three times independently.

Hemolytic activities of the peptides were measured by testing the hemoglobin release of h-RBCs in the presence of different peptides. h-RBCs from healthy volunteers were washed three times and suspended in PBS at 8% (v/v). 100 μL of 2-folded peptide solutions was added to wells in a sterile 96-well plate. Aliquots (100 μL) of the h-RBCs suspension was then added to the wells to give a total volume of 200 μL. The plate was incubated for 1 h at 37 °C, followed by centrifugation at 1000 *g* for 5 min. Aliquots (100 μL) of the supernatant was transferred to a new 96-well plate, and the hemoglobin release was monitored by measuring absorbance at 540 nm. The hemoglobin release values in PBS and 0.1% Triton X-100 were employed as the negative and positive controls.

2.4. Cell selectivity of G(IIKK)$_3$I-NH2

To assess the selective interaction of G(IIKK)$_3$I-NH$_2$ *in vitro*, FITC-G(IIKK)$_3$I-NH$_2$ was added into a co-culture system (8-well plate) containing primary cells (HDFa) and tumor cells (HL60) at the final peptide concentration of 20 μM. After incubation at 37 °C with 5% CO_2 for 1 h and appropriate separation procedures (See Ref. 8 for the detailed procedures), the peptide distribution in the two types of cells was observed with a Leica DMI3000 fluorescence microscopy.

2.5. Peptide penetration into different lipid monolayers

Penetration of the peptides into different lipid monolayers was followed in multi-well plate Kibron Microtrough X (Kibron Inc., Helsinki, Finland). Surface pressure (π) was monitored by using a Wilhelmy plate attaching to a Delta Pi microbalance (Kibron Inc., Helsinki, Finland). The lipid solution in chloroform was spread at the air-buffer interface (10 mM Tris–HCl, 154 mM NaCl, pH 7.4). After the solvent evaporation and the monolayer equilibration at different initial surface pressures (π_i, range from 10 to 40 mN/m), the peptide solution was injected beneath the monolayer, with the final peptide concentration of 3 μM in the subphase. The surface pressure was then monitored as a function of time and the equilibrated surface pressures (π_t) were obtained within 30 min. To compare the abilities of G(IIKK)$_3$I-NH$_2$ to penetrate into the saturated (DPPC) and unsaturated (POPC) phospholipid monolayers, the initial surface pressure was maintained around 30 mN/m. All measurements were performed at 20 ± 1 °C.

2.6. Location of G(IIKK)$_3$I-NH$_2$ in HeLa cells

HeLa cells (~1 × 10^5 cells/mL) were pre-seeded in a 6-well plate for 24 h and then FITC-G(IIKK)$_3$I-NH$_2$ was added to the wells with the final concentration of 10 μM. After incubation for 1 h or 24 h at 37 °C, the cells were washed with PBS at least three times. The distribution of FITC-G(IIKK)$_3$I-NH$_2$ in HeLa cells was observed using a Laser Confocal Microscope (Nikon AI-si).

2.7. Membrane integrity

HeLa cells (~1 × 10^5 cells/mL) were pre-seeded on a sterile 96-well plate for 24 h at 37 °C. The cells were washed with PBS and stained with Calcein-AM (1 μM) for 30 min at 37 °C. After washing with PBS three times, 100 μL PBS was added into each well and the fluorescence was recorded by the microplate autoreader (excitation at 490 nm and emission at 515 nm), with the obtained values as the control. Subsequently, these cells were treated with G(IIKK)$_3$I-NH$_2$ at a final peptide concentration of 10 μM for different times (10 min–6 h) at 37 °C. After the peptide treatment, the cells were washed three times with PBS and the fluorescence of the cells in the presence of 100 μL PBS was recorded again. Cells treated with PBS and 1% Triton X-100 were taken as the negative and positive controls, respectively.

To examine cell morphological changes, HeLa cells (~1 × 10^5 cells/mL) were pre-seeded on the coverslips under the bottom of the sterile 6-well plate for 24 h at 37 °C. The pre-seeded cells were treated with G(IIKK)$_3$I-NH$_2$ at a concentration of 10 μM for 24 h at 37 °C, and then the cells were washed twice with PBS and fixed with 4% paraformaldehyde for 15 min. The fixed cells were extensively washed with PBS and dehydrated with a gradation of ethanol concentrations. After critical-point drying and gold coating with a sputter coater, the samples were observed using a JSM-840 scanning electron microscope operated at 15 kV.

2.8. Fluorescence staining of F-actin, nucleus, mitochondria membrane potential and cytochrome c

For fluorescence staining, HeLa cells (~1 × 10^5 cells/mL) were pre-seeded in a 6-well plate for 24 h, followed by the addition of G(IIKK)$_3$I-NH$_2$ into the wells with a final concentration of 10 μM. After incubation for 24 h at 37 °C, the cells were washed with PBS and fixed with 4% paraformaldehyde for 15 min. The fixed cells were washed with PBS and were subjected to F-actin staining with FITC-phalloidin (5 μg/

mL) or nuclear staining with DAPI (6 μg/mL) for 30 min at 37 °C. After washing with PBS to remove unbound dyes, the stained cells were observed by fluorescence microscopy.

To follow the changes of the mitochondrial potential, the peptide treated HeLa cells (no fixing with 4% paraformaldehyde in this case) were stained with JC-1 (10 μg/mL) at 37 °C for 20 min. Then the stained cells were washed with PBS and observed with a fluorescence microscope.

The distribution of cytochrome c (Cyt c) in HeLa cells were obtained by immunofluorescence staining of Cyt c with anti-Cyt c monoantibody (mAb, mouse IgG2b). Briefly, after fixing with 4% paraformaldehyde, the peptide treated HeLa cells were permeabilized with 0.1% Triton X-100 for 5 min, followed by blocking with a blocking buffer (10% (v/v) fetal calf serum in PBS) for 30 min. After washing with PBS, these cells were incubated with anti-Cyt c mAb (1:50) at 37 °C for 1 h and washed with PBS for 5 min to remove the unbound antibody, followed by incubation with the FITC-labeled goat anti-mouse secondary antibody (1:100) for another 1 h. After washing extensively with PBS to remove the unbound secondary antibody, these cells were observed using the Laser Confocal Microscope. The peptide-untreated cells were used as the control in all the above fluorescence staining experiments.

2.9. Gel electrophoresis for DNA fragmentation

HeLa cells ($\sim 1 \times 10^6$ cells/mL) were pre-seeded in a sterile 6-well plate for 24 h. After incubation with 10 μM G(IIKK)$_3$I-NH$_2$ for different time interval (48, 24, 12 and 6 h) at 37 °C, HeLa cells were harvested and lysed with a lysis buffer (0.8% sodium dodecyl sulfate, 100 mM Tris–HCl, 20 mM EDTA, 0.15 mg/mL RNase A, pH8.0) at 37 °C for 2 h. After lysis, the lysates were incubated at 50 °C for further 24 h with 20 μL proteinase K (20 mg/mL), followed by the electrophoresis on 2% agarose gels containing 0.5 μg/mL ethidium bromide (EB).

2.10. RT-PCR (reverse transcription polymerase chain reaction and real time polymerase chain reaction)

To determine the related gene transcriptional activities about HeLa cell apoptosis and the lymphocyte immunological effects, RT-PCR assays were performed. Briefly, HeLa cells were incubated with 10 μM G(IIKK)$_3$I-NH$_2$ for different time intervals (1, 3, 6 and 12 h) and lymphocytes were incubated with 10 μM G(IIKK)$_3$I-NH$_2$ for 1 h. Total RNA from the cells was extracted by Trizol following the manufacturer's instructions (Invitrogen, Britain). Total RNA (1 μg) was subject to cDNA synthesis with random primers (PrimeScript Reverse Transcriptase, Takara, Japan). Real-Time PCR was performed with power SYBR green PCR Master Mix kit (Applied Biosystems, American) using a 7500 real-time PCR system (Applied Biosystems, American) according to the protocol of the manufacturer, and the data were analyzed by the relative quantitation of $2^{-\Delta\Delta Ct}$ method. Transcriptional levels of related genes were normalized to the values of house keeping gene β-actin. The following primers were used: β-actin sense: 5′-ATGCCAGGGTACATGGTGGT-3′, antisense: 5′-TCGTGCGTGACATTAAGGAG-3′; aspase-8 sense: 5′-ATGGACTTCAGCA GAAATCTT-3′, antisense: 5′-CATGTCATCATCCAGTTTGC-3′; fas sense: 5′-ATTATCGTCCAAAAGTGTTA-3′, antisense:5′-TCACACAATCTACATCTT CTG-3′; fas-L sense:5′-ATGCAGCAGCCCTTCAATT AC-3′, antisense: 5′-CAATCCTACCAAGG-CAACC-3′; IL2 sense: 5′-CACATTAACCTCAACTCC TGCCAC-3′, antisense:5′-CGTTGA-TATTGCTGATTAAGTCCCTG-3′; IL8 sense:5′- CGGAAGGAACCATCTCACTGTG-3′, antisense: 5′-AGAAATCAGGAAG GCTGCCAAG-3′.

2.11. Inhibition of tumor growth in human cervical carcinoma xenografts

Peptides including G(IIKK)$_3$I-NH$_2$ and G(IIKK)$_4$I-NH$_2$, denoted as 3# and 4# respectively, were dissolved in sterile PBS with two concentrations of 0.15 mg/mL and 0.5 mg/mL. 100 μL of human cervical carcinoma HeLa cells (2×10^6 cells/mL) in PBS were inoculated subcutaneously into the armpit of 5- to 6-week-old nude male mice (BALB/c-null) with an average weight of 20–25 g. When the tumor reached a mean volume of 100 mm^3 (5 days after inoculation), the mice were randomly divided into five groups (5 per group). 200–250 μL of the as-prepared peptide solutions were injected into the mice by intraperitoneal injection, with the final dosage 1.5 mg/kg or 5 mg/kg, and the injection of 200–250 μL PBS was also performed as negative control. Note that we define this day as day 0. The injection was carried out every other day for nine times. During the therapy, the tumor size and body weight of the mice were measured every two days. At day 18, the mice were sacrificed and the tumors were removed, photographed, and weighed.

3. Results

3.1. In vitro anticancer ability and selectivity

The G(IIKK)$_n$I-NH$_2$ ($n = 1$–4) peptides were synthesized via the Fmoc solid-phase peptide synthesis protocol [9–11]. CD studies revealed that these peptides existed predominantly in disordered structures in buffer solution. Upon addition into DPPG (dipalmitoyl phosphatidyl glycerol) SUVs (small unilamellar vesicles, mimicking the negatively charged bacterial and cancer cell membranes), the peptides adopted α-helical conformations except for GIIKKI-NH$_2$. The amphipathic helical structure favored their interactions with the lipid bilayers, but GIIKKI-NH$_2$ always remained unfolded irrespective of any changes in the surrounding environment. This lack of changes in the secondary structure was well consistent with its lack of bioactivity. Subsequent cell studies focused on the series with $n = 2$, 3 and 4.

Following a concentration-dependent pattern, the peptides with more repeats or longer length were more effective in killing cancer cells (HeLa and HL60 cells), but the *in vitro* toxicity to normal cells (erythrocytes and HDFa cells) also started to increase, as shown in Fig. 1a–c. Overall, G(IIKK)$_3$I-NH$_2$ was the optimal sequence in terms of *in vitro* anticancer activity and cell selectivity, with its IC_{50} values being 15 and 25 μM against HeLa and HL60 cells and EC_{50} being far more than 250 μM (IC_{50}: concentration causing 50% cancer cell growth inhibition; EC_{50}: concentration to induce 50% lysis of erythrocytes). Importantly, these peptides are well tolerated by HDFa cells, for example, inconsiderable impact of G(IIKK)$_3$I-NH$_2$ to the HDFa cells at concentrations below 50 μM (Fig. 1c). Such performance of our rationally designed short peptides is clearly advantageous over natural AMPs such as magainin and melittin and is also better than anticancer drug cisplatin in terms of effectiveness, selectivity and even resistance [12–15]. For example, under similar experimental conditions, magainin-2 offered a less attractive IC_{50} of more than 60 μM against HeLa cells whilst melittin offered a far lower EC_{50} under 5 μM, showing high toxicity to the host cells [12–14].

Then, we further assessed the cell selectivity based on an *in vitro* co-culture system containing both HL60 cancer cells and HDFa primary cells, which closely mimic the *in vivo* environment [8]. FITC-G(IIKK)$_3$I-NH$_2$ was added into the system with the final concentration of 20 μM and after incubation for 1 h, the peptide distribution in the two types of cells was followed by fluorescence microscopy (Fig. 1d). It is evident that the green fluorescence was concentrated in the suspended and rounded HL60 cells rather than the adherent and spindle HDFa cells, indicating again excellent cell selectivity of the peptide, as well as its rapid recognition of cancer cells.

3.2. Selective interaction of peptides with lipid monolayers

The mechanistic processes underlying the selectivity of these peptides remain largely unclear at this stage, but anticancer peptides are mostly membrane-active and their mode of action against cancer cells involves membrane disruption. Moreover, their selective killing of cancer cells is intimately related to two key cell membrane hallmarks of cancer cells, i.e., net negative surface charges and greater membrane fluidity [2,3,16]. To understand the specific interaction between peptides and cell membranes and fundamental process of anticancer action at the molecular level, we turned to membrane models using lipid monolayers. Fig. 2a shows the surface pressure increases ($\Delta\pi$) of the DPPC (dipalmitoyl phosphatidylcholine) and DPPG monolayers (mimicking normal mammalian host cell and cancer cell outer membranes, respectively) from different initial surface pressures (π_i) upon injection of G(IIKK)$_{(2-4)}$I-NH$_2$ into the subphase at a final concentration of 3 μM whilst maintaining the surface area constant. All peptides exhibited a clear preference to the negatively charged DPPG monolayer while a far less extent of affinity to the zwitterionic DPPC monolayer was noted. Extrapolation of each pressure plot at $\Delta\pi = 0$ yields the exclusion pressure, above which the peptide is no longer able to penetrate the lipid monolayer to cause further surface pressure increase. For the zwitterionic DPPC monolayer, G(IIKK)$_2$I-NH$_2$ had an exclusion pressure of 23.4 mN/m, well below the physiological range of 30–35 mN/m for biological membranes [17,18], in good

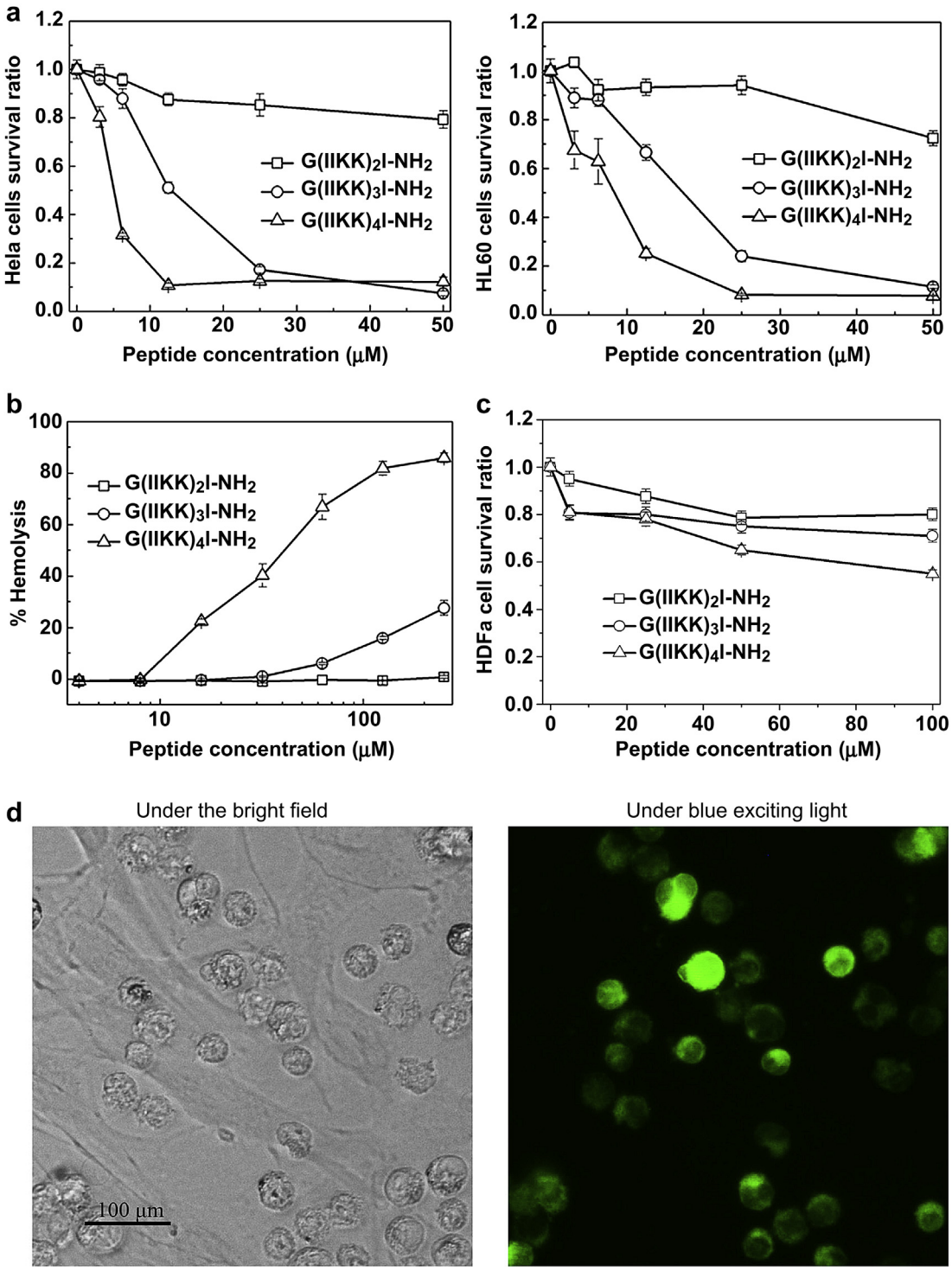

Fig. 1. Cytotoxicity and selectivity of the designed α-helical peptides. (a) Cytotoxicity against HeLa and HL60 cells. (b) Human red blood cell hemolysis. (c) Cytotoxicity against HDFa cells. (d) The distribution of FITC-G(IIKK)$_3$I-NH$_2$ in an *in vitro* co-culture system containing HL60 cancer cells and HDFa primary cells.

line with its little toxicity against erythrocytes. In contrast, G(IIKK)$_{(3-4)}$I-NH$_2$ showed increased values to 32.0 and 37.6 mN/m, respectively, consistent with their increased hemolytic activities. For the negatively charged DPPG monolayer, on the other hand, the exclusion pressure had increased significantly to 37.3, 40.6 and 42.6 mN/m, respectively, indicating the crucial role of the electrostatic interaction between the cationic peptide charges and the anionic lipid head groups. Despite a larger exclusion pressure difference between DPPC and DPPG monolayers for G(IIKK)$_2$I-NH$_2$ (see Supplementary Data, Fig. S1), its exclusion pressure against the latter is only slightly higher than the physiological range of 30–35 mN/m for biological membranes, consistent with its lower efficiency in killing cancer cells, thus making the peptide unattractive in cancer therapy. On the other hand, G(IIKK)$_4$I-NH$_2$ exhibited the exclusion pressure of 37.6 mN/m against the zwitterionic DPPC monolayer slightly above the physiological range of 30–35 mN/m,

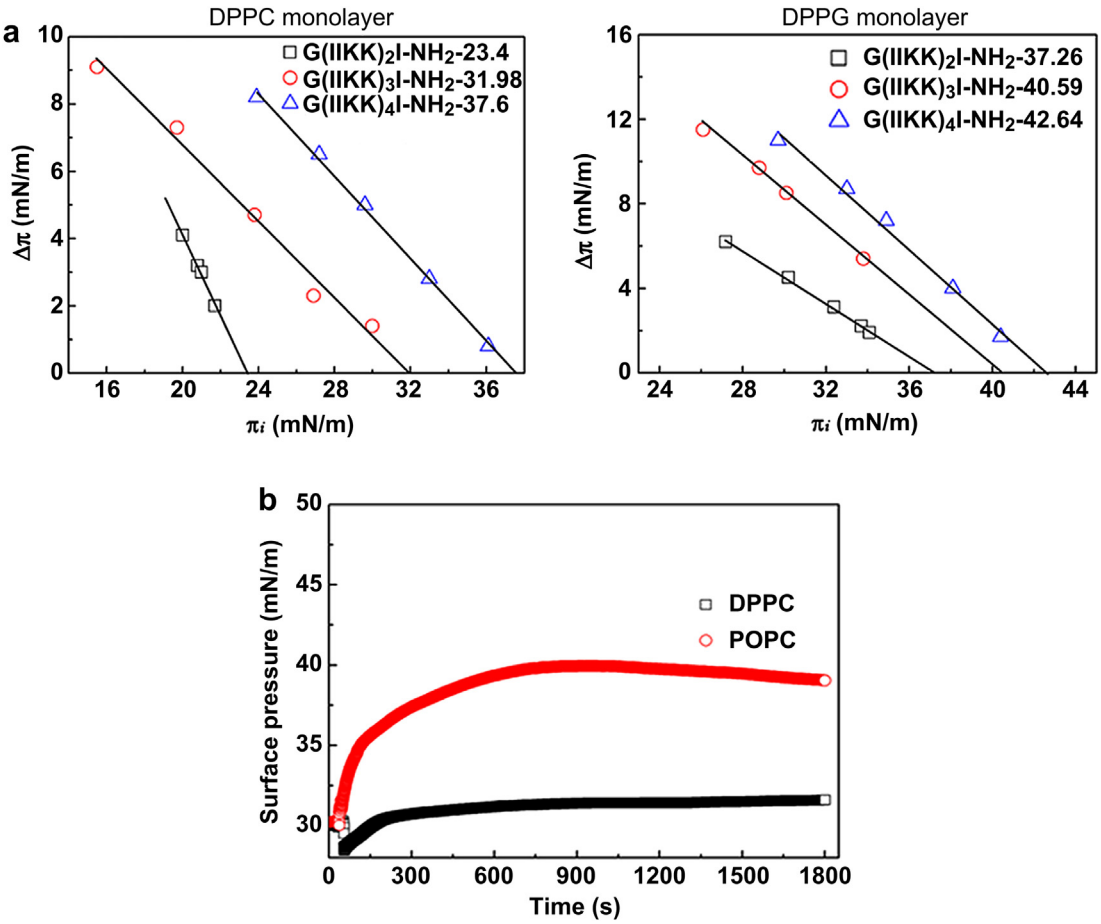

Fig. 2. Interaction of the peptides with different lipid monolayers. (a) Surface pressure increase ($\Delta\pi$) of the DPPC and DPPG monolayers at different initial surface pressures (π_i) upon peptide injection into the subphase at the concentration of 3 μM. (b) Surface pressure against time following the injection of G(IIKK)$_3$I-NH$_2$ into the subphase of the DPPC and POPC monolayers.

consistent with its display of the highest hemolytic ability in the series. G(IIKK)$_3$I-NH$_2$ showed the intermediate values, with the $\Delta\pi$ values of 32.0 mN/m against the DPPC monolayer and of 40.6 mN/m for the DPPG monolayer, consistent with its best cell selectivity in the *in vitro* cell work.

The decrease of cholesterol level and the increase of lipids possessing unsaturated fatty acyl chains in cancer cells may account for the increased membrane fluidity [19]. After injection of G(IIKK)$_3$I-NH$_2$ into the subphase with a final concentration of 3 μM, the equilibrated surface pressure increases tended to 3.5 and 10 mN/m for the saturated DPPC and unsaturated palmitoyl-oleoyl-phosphatidylcholine (POPC) monolayers with the initial surface pressure at 30 mN/m (Fig. 2b), indicating that the increased membrane fluidity did favor the membrane penetration of surface active peptides, irrespective of the membrane charge interaction.

3.3. *In situ peptide location and plasma membrane integrity*

To precisely locate anticancer peptides during incubation with HeLa cells, FITC-G(IIKK)$_3$I-NH$_2$ was used at a concentration of 10 μM and its fluorescence distribution in these cells was visualized using laser confocal microscopy, with respect to incubation time. After 1 h of incubation, majority of FITC-derived signals (green (in the web version)) were located at the HeLa cell membrane and relatively weak fluorescent signals were observed within the cytoplasm (Fig. 3a), indicating that the membranes surrounding the cells are the primary targets during this period. After 24 h of incubation, however, fluorescent signals accumulated inside cells (Fig. 3b), indicating the translocation of the peptide across the outer lipid bilayers. Furthermore, the cell boundary after 24 h of treatment became markedly blurry, presumably due to the gradual structural deterioration of cell membranes during this process. It is thus well expected that after translocation, the peptide would interact with intracellular targets, such as mitochondria, triggering cell apoptosis.

To determine membrane permeability after binding with the peptide, we performed the Calcein-AM release assay. Incubation with 10 μM G(IIKK)$_3$I-NH$_2$ for 10 min resulted in some 20% Calcein-AM release from HeLa cells, indicating its rapid permeabilizing effect on the cancer cell membranes (see Supplementary Data, Fig. S2). As expected, increasing the incubation time led to more membrane permeabilization and more than 40% Calcein-AM release was achieved after 6 h of incubation. The obvious membrane permeabilization within shorter incubation time is well consistent with the rapid binding of the peptide to cancer cell membranes observed above.

To directly observe the effect of G(IIKK)$_3$I-NH$_2$ on cell morphology, particularly after longer incubation time when most of the peptide molecules transferred across the membrane, we then performed SEM examination. Untreated HeLa cells showed a normal smooth surface, with good cell–cell contacts among neighboring cells (Fig. 3c). In contrast, HeLa cells treated with 10 μM G(IIKK)$_3$I-NH$_2$ for 24 h exhibited marked alterations in cell morphology (Fig. 3d). The shrunken cells with significant

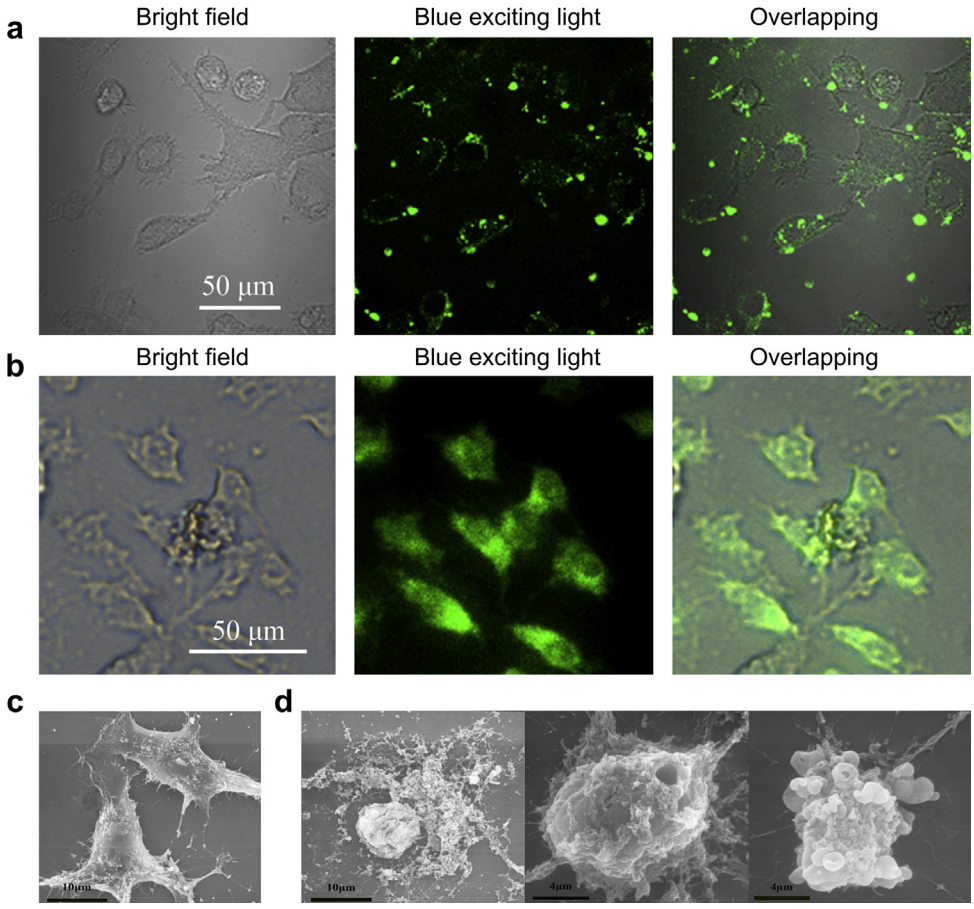

Fig. 3. *In situ* peptide localization and plasma membrane integrity. (a) Peptide location in HeLa cells following their incubation with 10 μM FITC-G(IIKK)$_3$I-NH$_2$ for 1 h. (b) Peptide location in HeLa cells following their incubation with 10 μM FITC-G(IIKK)$_3$I-NH$_2$ for 24 h. (c) Representative SEM micrograph of HeLa cells untreated. (d) Representative SEM micrographs of HeLa cells treated with 10 μM G(IIKK)$_3$I-NH$_2$ for 24 h.

membrane disruption and lysis were observed. Apart from cell membrane damage, some treated cells exhibited severe surface blebbing (the right image of Fig. 3d), a characteristic event during the execution phase of cell apoptosis [20].

3.4. Cell apoptosis

Because of the peptide translocation into the cytoplasm and the occurrence of apoptotic morphology with the treated cancer cells, we then followed several key biochemical and morphological hallmarks of cell apoptosis, with the intention of correlating the induction of apoptosis with the HeLa cell death and unraveling possible apoptotic pathways.

3.4.1. Nuclear morphological change and DNA fragmentation

Chromatin condensation paralleled by DNA fragmentation is a reliable criterion used to identify cell apoptosis [21]. By staining cells with DAPI, we first compared the nuclear change of HeLa cells before and after 24 h of treatment with 10 μM G(IIKK)$_3$I-NH$_2$ at 37 °C (Fig. 4a). The nuclear morphology of untreated HeLa cells was regular and intact with diffuse DAPI staining. In contrast, the shape of peptide-treated cell nuclei was changed and the chromatin aggregated into irregular compact clumps with increasing fluorescence intensity. Furthermore, genomic DNA was extracted from the treated HeLa cells at varying incubation time and then analyzed by the agarose gel electrophoresis. After 12 h of incubation, oligonucleosome-sized DNA fragments appeared and the pattern became more distinguished with increasing incubation time (Fig. 4b). In contrast, the band of DNA isolated form untreated HeLa cells was single, without the occurrence of DNA fragmentation. It has been proposed that some activated enzymes such as endogenous nucleases were responsible for the cleavage of chromatin DNA into fragments of 180–200 bp and integer multiples thereof [22–24] once the chromatin integrities were compromised.

3.4.2. Cytoskeleton alteration

The actin cytoskeleton plays a crucial role in mediating cell responses to both internal and external signals [25]. It has a dynamic structure with distinct forms suitable for particular tasks such as motility, adhesion, division and cell death [26–28]. The occurrence of aberrant F-actin dynamics is closely linked with the development of cell apoptosis and usually accompanied by the mitochondrial release of ROS [28]. Before and after their incubation with 10 μM G(IIKK)$_3$I-NH$_2$, HeLa cells were stained with FITC-phalloidin to visualize F-actins (filamentous actins). For untreated cells, fine microfilament bundles were oriented parallel to the long axes of cells while F-actins became disordered and shortened with treated cells (Fig. 4c).

3.4.3. Mitochondrial pathway

Mitochondrion plays a central part in cell apoptosis and many crucial factors and events in apoptotic death are regulated by it. Some apoptotic proteins can target on mitochondria, leading to either mitochondrial swelling via the formation of membrane pores

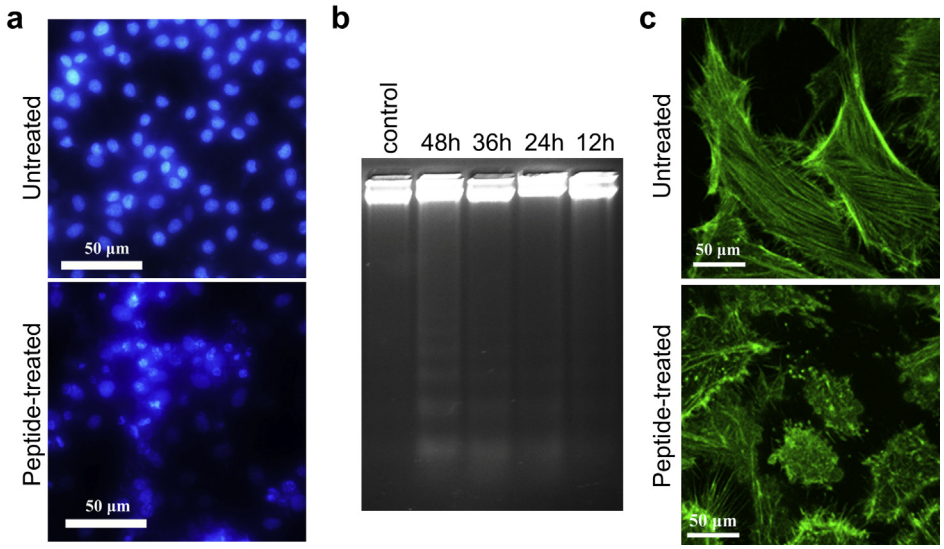

Fig. 4. Biochemical and morphological characteristics of cell apoptosis. (a) Nuclear staining with DAPI of HeLa cells before and after incubation with 10 μM $G(IIKK)_3I\text{-}NH_2$ for 24 h. (b) The gel electrophoresis analysis of genomic DNA extracted from HeLa cells following their incubation with 10 μM $G(IIKK)_3I\text{-}NH_2$. (c) F-actin staining with FITC-phalloidin of HeLa cells before and after incubation with 10 μM $G(IIKK)_3I\text{-}NH_2$ for 24 h.

or increasing mitochondrial membrane permeability. Both processes allow the release of apoptotic effectors [29–32]. In this work, mitochondrial pathway was successfully observed to be responsible for cell apoptosis. We first followed changes in mitochondrial membrane potential using JC-1 as a probe [33]. Untreated HeLa cells displayed mitochondrial orange-red fluorescence with little green (in the web version) fluorescence. After 24 h of incubation with 10 μM $G(IIKK)_3I\text{-}NH_2$, green fluorescence dominated (Fig. 5a), indicating a significant loss of mitochondrial membrane potential. This depolarization in mitochondrial membrane potential is often accompanied with increasing mitochondrial membrane permeability and Cyt c release [34]. We then took immuno-fluorescence imaging which showed a clear, grainy staining pattern for Cyt c in untreated cells, in contrast to more diffuse staining of Cyt c in the $G(IIKK)_3I\text{-}NH_2$ treated cells (Fig. 5b). The difference indicated the release of Cyt c from mitochondria to the cytosol, highly consistent with the observed depolarization of mitochondrial membrane potential. In cytosol, the released Cyt c could induce the interaction between Apaf-1 and caspase-9 in the presence of dATP, which could further activate caspase cascade reaction and trigger cell apoptosis [35].

3.4.4. Death receptor pathway

The cell apoptosis regulated by mitochondria can be amplified by other receptor related pathways such as the interaction of Fas and its ligand (Fas-L) [36]. To investigate if the peptide initiated the death receptor pathway, we performed a real-time PCR assay to analyze the related gene transcriptions (caspase-8, fas and fas-L). The caspase-8 transcriptional level of HeLa cells treated with 10 μM $G(IIKK)_3I\text{-}NH_2$ from 3 to 6 h showed an obvious increase, whereas it sharply decreased to the normal value after 12 h of incubation. The transcription of fas and fas-L followed the same trend (Fig. 5c). The high expression of the two genes (fas and fas-L) increased the chance of their interaction. The binding of the two molecules induced the formation of the death-inducing signaling complexes (DISC), which contained caspase-8 and caspase-10 [36,37]. The Fas-DISC started a feedback loop that spiraled into increasing the release of pro-apoptotic factors from mitochondria and the amplified activation of caspase-8 [38]. On the other hand, caspase-8 induced apoptosis could also be amplified through stimulating the mitochondrial release of Cyt c [39]. The high transcriptions of death receptor pathway genes in the $G(IIKK)_3I\text{-}NH_2$ treated HeLa cells imply that the cell apoptosis induced by the peptide also involved the death receptor dependent manner.

3.5. Immunological effects

Natural antibacterial peptides isolated from living organisms are very limited in clinical use because of their high production cost, high hemolysis and possible immunological effects [16]. Apart from low production cost and low hemolytic action through high cell selectivity, the non-immunological effects of the designed helical peptides are also essential for developing their potential applications. Two cytokine genes, IL2 and IL8, are regarded as the major immune system signal molecules that are able to response to the microbial infection and discriminate foreign molecules (non-self) from the body's own cells and molecules (self) in human body [40,41]. As a result, high expression of the two genes typically induces the acute and chronic inflammation. Thus, the transcriptional levels of the cytokine genes IL2 and IL8 of human lymphocytes were analyzed using RT-PCR assay, after their treatment with the peptide $G(IIKK)_3I\text{-}NH_2$. As shown in Fig. S3, the relative transcriptional levels of IL2 and IL8 of lymphocytes following the peptide incubation was lower or almost equal to those of the respective controls, indicating that the interaction of $G(IIKK)_3I\text{-}NH_2$ with lymphocytes did not induce non-specific immunogenic responses.

3.6. In vivo antitumor performance

Human cervical carcinoma HeLa cells were inoculated s.c. in nude mice. 5 days after tumor implantation, the peptides $G(IIKK)_3I\text{-}NH_2$ and $G(IIKK)_4I\text{-}NH_2$ were injected intraperitoneally respectively, at doses of 1.5 mg/kg and 5 mg/kg. During the administration, no signs of toxicity such as body weight loss and poor appearance were observed (Fig. 6b), although $G(IIKK)_4I\text{-}NH_2$ showed higher *in vitro* hemolysis. In comparison with the negative control in PBS, the two peptides showed noticeable inhibition on the tumor growth, with $G(IIKK)_4I\text{-}NH_2$ exhibiting better efficacy than $G(IIKK)_3I\text{-}NH_2$ (Fig. 6c), consistent with their *in vitro* antitumor trend. 18 days later, tumors were dissected out and weighed (Fig. 6a and d). The tumor growth inhibition rates calculated for the groups treated with $G(IIKK)_3I\text{-}NH_2$ at doses of 1.5 mg/kg and 5 mg/kg were

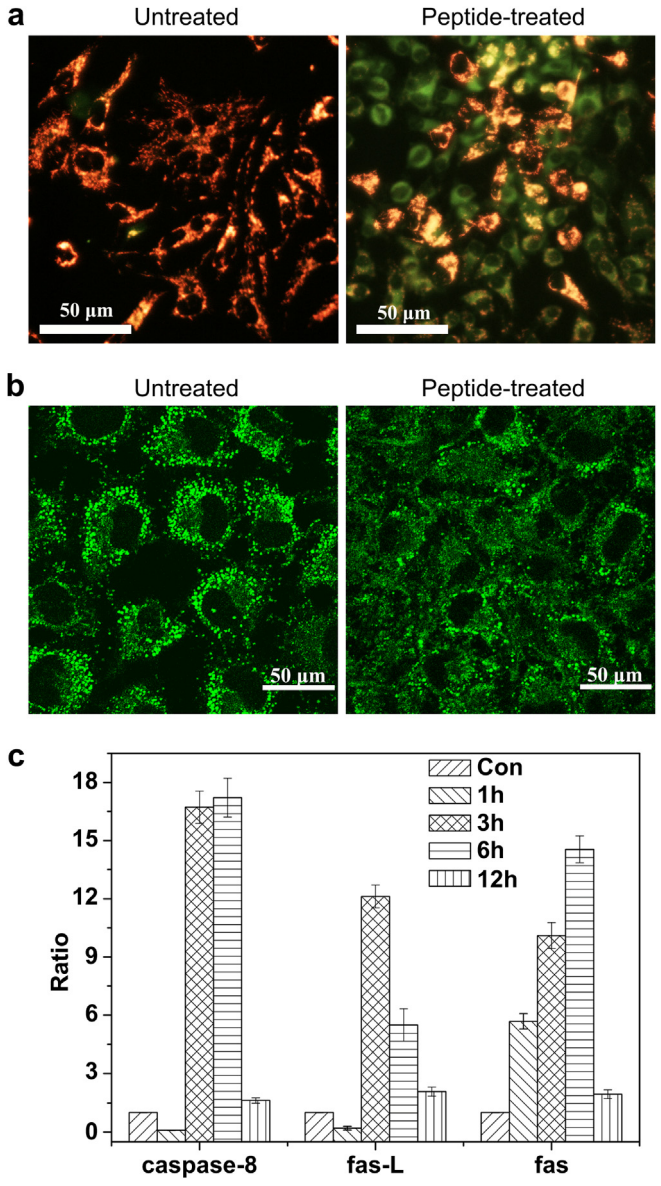

Fig. 5. Mitochondrial dysfunction and Fas-FasL pathway. (a) Fluorescent images of mitochondrial membrane potential staining with JC-1 of HeLa cells before and after incubation with 10 μM $G(IIKK)_3I\text{-}NH_2$ for 24 h. (b) Immuno-fluorescence staining of Cyt c of HeLa cells before and after incubation with 10 μM $G(IIKK)_3I\text{-}NH_2$ for 24 h. (c) Caspase-8, fas-L and fas gene transcriptions of HeLa cells after incubation with 10 μM $G(IIKK)_3I\text{-}NH_2$.

0.23 and 0.31, respectively. $G(IIKK)_4I\text{-}NH_2$ resulted in more effective inhibition, with the rates of 0.32 and 0.41 at doses of 1.5 mg/kg and 5 mg/kg, respectively. These data suggest that the helical peptides can effectively inhibit tumor growth in the mice xenograft model, while the tumor cells could not be completely eradicated. The incomplete inhibition effect has been widely observed for many antitumor agents, which can be ascribed to a variety of mechanisms such as relatively fast clearance of agents from the tumor sites and their difficulties to diffuse through the necrotic area [42], but the precise reasons behind the current group of peptides await for further mechanistic investigation.

4. Discussion

These designed peptides are short and regular. Their simple structure together with high potency and little side effects compared to the typical natural AMPs and popular anticancer drug cisplatin in inhibiting cancer cell growth makes them ideal models and targets for fundamental and applied research. The peptides display systematic changes in their interfacial property and bioactivity. Our immediate challenge lies in correlating molecular structural design, interfacial property with the selectivity in disrupting cell membranes. This represents the core endeavor of functional biomaterials research leading to better molecular insight in the rational design of future peptide antibiotics and the understanding of their antitumor performance.

Our previous studies using NIH 3T3 cell line as host cells under the co-culturing environment have illustrated a broadly similar pattern of action of these peptides against bacteria and cancer cells and explained why they do not cause harm to normal mammalian cells [8]. Because of the elevated expressions of phosphatidylserine, O-glycosylated mucins, sialiated gangliosides and heparin sulfates, tumor cell membranes also carry the net negative charges. This negative charge feature of the outer membrane surfaces is very similar to that of bacteria. The electrostatic interaction between these peptides and target membranes must be crucial to the selective responses.

In the short designed peptide series studied, $G(IIKK)_3I\text{-}NH_2$ represents the optimal chain length in terms of *in vitro* anticancer activities and cell selectivity, consistent with the observations in antimicrobial activity and selectivity reported previously. The common discriminative responses to bacterial and cancer cells have been shown to originate from the selective responses of the peptides to different cell membranes through the balance between electrostatic interaction and hydrophobic effect. Specifically, the high affinity to cancer cells driven by the negative surface charges and highly unsaturated lipid chains leads to the rapid binding of $G(IIKK)_3I\text{-}NH_2$ to cancer cell membranes and the subsequent membrane permeabilization. The peptide molecules subsequently translocate across lipid bilayers and become accumulated in the interior of the cancer cells. This process produces a series of morphological and biochemical hallmarks of cell apoptosis signifying the death of peptide-treated cancer cells arising from membrane disruption and apoptosis. Furthermore, this work has revealed that the peptide induced apoptosis in cancer cells is associated with the two characteristic molecular processes: the mitochondrial pathway and the death receptor pathway.

The peptides are shown not to induce non-specific immunogenic responses after interacting with lymphocytes and importantly, they show considerable *in vivo* growth inhibitory effects on xenografts in nude mice with little toxicity to the hosts, thus indicating their huge potential in clinical development. These data together form a basis for a new paradigm in designing short peptide biomaterials with exceptional biocompatibility and selectivity. Many AMPs as reported so far emphasize the biomimicry by taking amino acid sequences from natural proteins and peptides. In contrast, in the present work we adopt the minimum mimicry of the basic unit of the IIKK sequence module and then adopt artificial repeats (n) and selective terminal blocking, resulting in substantially improved performance. Future work could assess how biomimicry is reconciled with rational structural design. It remains unclear how changes in the primary sequence, e.g., replacing I by L, V and A, or K by R and any unnatural cationic amino acids with short side chains would alter potency and selectivity.

On the other hand, although the selective responses of the short peptides to different cell types conform to the experimental observations, cell outer membrane surfaces are elaborate and complex. The current explanation on the basis of selective electrostatic interactions could at best be a simplified rationalization. Further studies are necessary to unravel the detailed molecular processes through different levels of model interfacial representations,

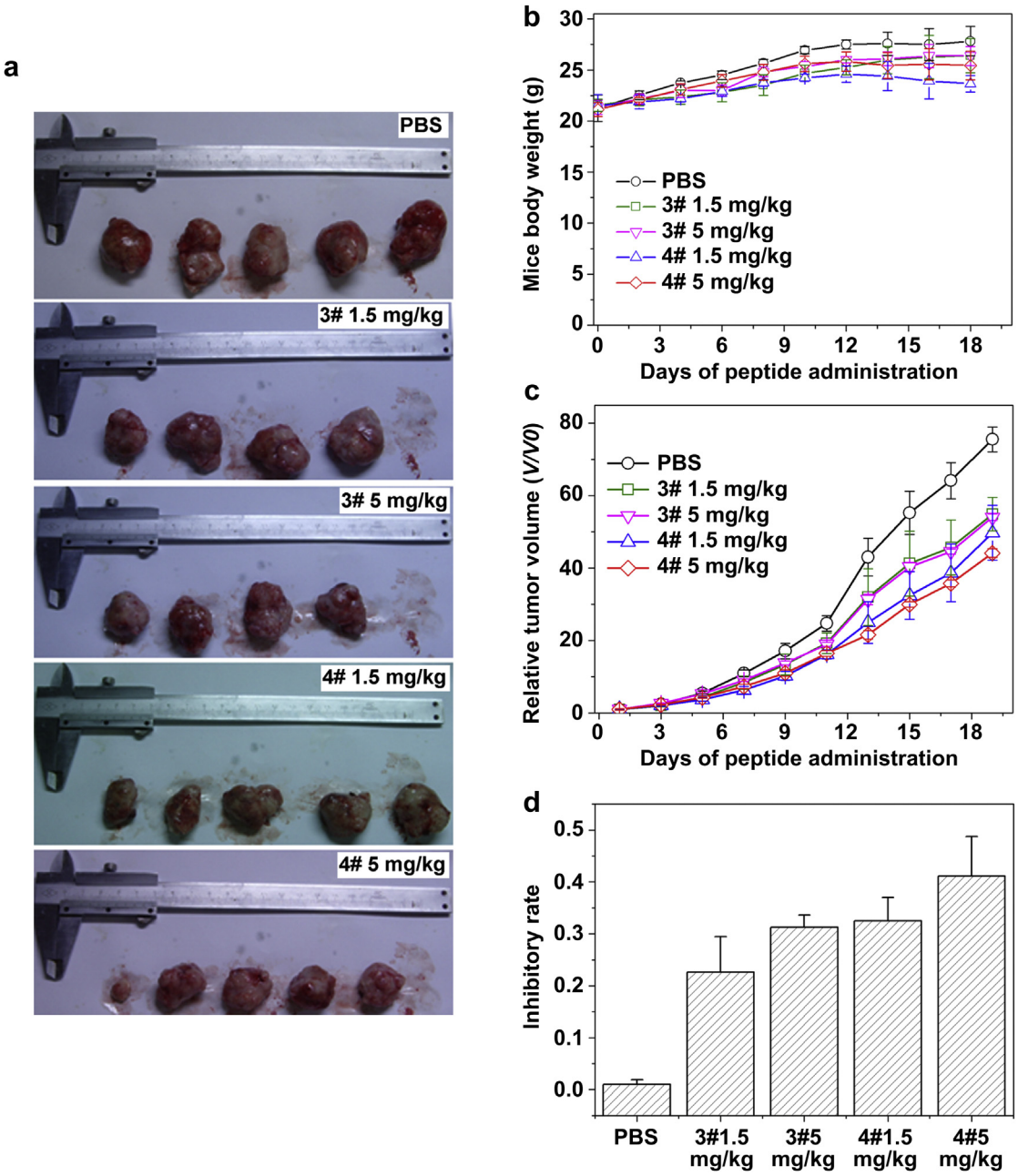

Fig. 6. *In vivo* antitumor effects on human cervical carcinoma xenografts in nude mice. (a) Dissected tumors after the administration. (b) Body weight variations during the administration. (c) The variations in tumor volume during the administration. (d) The tumor inhibition rates after the administration.

providing more direct insight in different interactions at different cellular and sub-cellular interfaces. The current work thus opens up a wide range of challenging and yet exciting experimental opportunities for exploring new scientific understanding. The development of relevant model biointerfaces in conjunction with short designed functional peptides will facilitate new experimental capabilities including various surfaces and interfacial imaging, reflection and scattering using lasers, x-ray and neutron beam sources. These experiments will not only add new understanding of biointerfacial processes but also spring off new technologies.

Finally, previous studies have revealed that surfactant-like short peptides such as A_9K also show high potency and selectivity in cancer growth inhibition [11], but these peptides promoted β-sheet conformation in water and under membrane-like milieu, instead of the α-helical conformation as reported in this work. It remains unclear how different secondary structures could lead to equivalently high potency and selectivity, but having well defined molecular structures lays a useful foundation for us to look into these important differences in future research. For physicists and materials researchers undertaking interdisciplinary studies, these rationally designed models are better to handle than the diverse range of natural AMPs and homologues reported already. Regardless of the directions of the debate and outcome, these short peptides will raise a huge range of interests to explore their functional uses. Changes in potency have different implications. For example, very short peptides could be applied to skincare whilst longer ones with greater potency could be targeted to therapeutic development.

5. Conclusion

In the series of the short designed peptides $G(IIKK)_nI\text{-}NH_2$ ($n = 1–4$), $G(IIKK)_3I\text{-}NH_2$ represents the optimal chain length in terms of *in vitro* anticancer activities and cell selectivity, consistent with the previous observations in antimicrobial activity and selectivity. The common discriminative response to bacterial and cancer cells have been shown to originate from the selective response of the peptides through the balance between electrostatic interaction and hydrophobic effect. Specifically, the high affinity driven by the negative surface charges and high unsaturated lipid chains leads to the rapid binding of $G(IIKK)_3I\text{-}NH_2$ to cancer cell membranes and the subsequent membrane permeabilization. The peptide molecules then translocate across lipid bilayers and become accumulated in the interior of the cancer cells. This process produces a series of morphological and biochemical hallmarks of cell apoptosis signifying the death of peptide-treated cancer cells arising from membrane disruption and apoptosis. Furthermore, this work has revealed that the peptide induced apoptosis in cancer cells is associated with the two characteristic molecular processes: the mitochondrial pathway and the death receptor pathway. Finally, the peptide is shown not to induce non-specific immunogenic responses after interacting with lymphocytes and importantly, these designed peptides show considerable *in vivo* antitumor effect in xenograft models while with little toxicity, both indicating their potential in biotechnological and clinical applications as functional materials.

Acknowledgments

This work was supported by the National Natural Science Foundation of China under grant numbers 31271497, 30900765 and 21033005, the Natural Science Foundation of Shandong Province (ZR2009DQ001 and JQ201105), and the Fundamental Research Funds for the Central Universities (12CX04052A). We also thank the UK Engineering and Physical Sciences Research Council (EPSRC) for support. We thank the Royal Society (London) for a Sino-British Fellowship for HX.

Appendix A. Supplementary data

Supplementary data related to this article can be found online at http://dx.doi.org/10.1016/j.biomaterials.2013.10.082.

References

[1] Jemal A, Siegel R, Xu J, Ward E. Cancer statistics, 2010. CA Cancer J Clin 2010;60:277–300.
[2] Schweizer F. Cationic amphiphilic peptides with cancer-selective toxicity. Eur J Pharmacol 2009;625:190–4.
[3] Hoskin DW, Ramamoorthy A. Studies on anticancer activities of antimicrobial peptides. BBA-Biomembranes 2008;1778:357–75.
[4] Mader JS, Hoskin DW. Cationic antimicrobial peptides as novel cytotoxic agents for cancer treatment. Expert Opin Investig Drugs 2006;15:933–46.
[5] Dathe M, Wieprecht T. Structural features of helical antimicrobial peptides: their potential to modulate activity on model membranes and biological cells. BBA-Biomembranes 1999;1462:71–87.
[6] Zelezetsky I, Tossi A. Alpha-helical antimicrobial peptides-using a sequence template to guide structure–activity relationship studies. BBA-Biomembranes 2006;1758:1436–49.
[7] Giangaspero A, Sandri L, Tossi A. Amphipathic alpha helical antimicrobial peptides. Eur J Biochem 2001;268:5589–600.
[8] Hu J, Chen C, Zhang S, Zhao X, Xu H, Zhao X, et al. Designed antimicrobial and antitumor peptides with high selectivity. Biomacromolecules 2011;12:3839–43.
[9] Xu H, Wang J, Han S, Wang J, Yu D, Zhang H, et al. Hydrophobic region induced transitions in self-assembled peptide nanostructures. Langmuir 2009;25:4115–23.
[10] Chen C, Pan F, Zhang S, Hu J, Cao M, Wang J, et al. Antibacterial activities of short designer peptides: a link between propensity for nanostructuring and capacity for membrane destabilization. Biomacromolecules 2010;11:402–11.
[11] Chen C, Hu J, Zhang S, Zhou P, Zhao X, Xu H, et al. Molecular mechanisms of antibacterial and antitumor actions of designed surfactant-like peptides. Biomaterials 2012;33:592–603.
[12] Cruciani RA, Barker JL, Zasloff M, Chen HC, Colamonici O. Antibiotic magainins exert cytolytic activity against transformed cell lines through channel formation. Proc Natl Acad Sci U S A 1991;88:3792–6.
[13] Asthana N, Yadav SP, Ghosh JK. Dissection of antibacterial and toxic activity of melittin: a leucine zipper motif plays a crucial role in determining its hemolytic activity but not antibacterial activity. J Biol Chem 2004;279:55042–50.
[14] Baker MA, Maloy WL, Zasloff M, Jacob LS. Anticancer efficacy of magainin2 and analogue peptides. Cancer Res 1993;53:3052–7.
[15] Florea AM, Büsselberg D. Cisplatin as an anti-tumor drug: cellular mechanisms of activity, drug resistance and induced side effects. Cancers 2011;3:1351–71.
[16] Papo N, Shai Y. Host defense peptides as new weapons in cancer treatment. Cell Mol Life Sci 2005;62:784–90.
[17] Brockman H. Lipid monolayers: why use half a membrane to characterize protein-membrane interactions? Curr Opin Struct Biol 1999;9:438–43.
[18] Marsh D. Lateral pressure in membranes. BBA-Rev Biomembranes 1996;1286:183–223.
[19] Hendrich AB, Michalak K. Lipids as a target for drugs modulating multidrug resistance of cancer cells. Curr Drug Targets 2003;4:23–30.
[20] Kerr JFR, Wyllie AH, Currie AR. Apoptosis: a basic biological phenomenon with wide-ranging implications in tissue kinetics. Br J Cancer 1972;26:239–57.
[21] Oberhammer FA, Hochegger K, Fröschl G, Tiefenbacher R, Pavelka M. Chromatin condensation during apoptosis is accompanied by degradation of lamin A+B, without enhanced activation of cdc2 kinase. J Cell Biol 1994;126:827–37.
[22] Walker PR, Kokileva L, Leblanc J,Sikorska M. Detection of the initial stages of DNA fragmentation in apoptosis. Biotechniques 1993;15:1032–40.
[23] Bortner CD, Oldenburg NBE, Cidlowski JA. The role of DNA fragmentation in apoptosis. Trends Cell Biol 1995;5:21–6.
[24] Saraste A, Pulkki K. Morphologic and biochemical hallmarks of apoptosis. Cardiovasc Res 2000;45:528–37.
[25] Gourlay CW, Ayscough KR. The actin cytoskeleton: a key regulator of apoptosis and ageing? Nat Rev Mol Cell Biol 2005;6:583–9.
[26] Rangel M, Prado MP, Konno K, Naoki H, Freitas JC, Machado-Santelli GM, et al. Cytoskeleton alterations induced by *Geodia corticostylifera* depsipeptides in breast cancer cells. Peptides 2006;27:2047–57.
[27] Ndozangue-Touriguine O, Hamelin J, Bréard J. Cytoskeleton and apoptosis. Biochem Pharmacol 2008;76:11–8.
[28] Gourlay CW, Ayscough KR. A role for actin in aging and apoptosis. Biochem Soc Trans 2005;33:1260–4.
[29] Green DR, Reed JC. Mitochondria and apoptosis. Science 1998;281:1309–12.
[30] Desagher S, Martinou JC. Mitochondria as the central control point of apoptosis. Trends Cell Biol 2000;10:369–77.
[31] Li H, Kolluri SK, Gu J, Dawson MI, Cao X, Hobbs PD, et al. Cytochrome c release and apoptosis induced by mitochondrial targeting of nuclear orphan receptor TR3. Science 2000;289:1159–64.
[32] Ly JD, Grubb DR, Lawen A. The mitochondrial membrane potential ($\Delta\psi$ m) in apoptosis; an update. Apoptosis 2003;8:115–28.
[33] Smiley ST, Reers M, Mottola-Hartshorn C, Lin M, Chen A, Smith TW, et al. Intracellular heterogeneity in mitochondrial membrane potentials revealed by a J-aggregate-forming lipophilic cation JC-1. Proc Natl Acad Sci U S A 1991;88:3671–5.
[34] Heiskanen KM, Bhat MB, Wang HW, Ma J, Nieminen AL. Mitochondrial depolarization accompanies cytochrome c release during apoptosis in PC6 cells. J Biol Chem 1999;274:5654–8.
[35] Li P, Nijhawan D, Budihardjo I, Srinivasula SM, Ahmad M, Alnemri ES, et al. Cytochrome c and dATP-dependent formation of Apaf-1/caspase-9 complex initiates an apoptotic protease cascade. Cell 1997;91:479–89.
[36] Ashkenazi A, Dixit VM. Death receptors: signaling and modulation. Science 1998;281:1305–8.
[37] Kavurma M, Khachigian L. Signaling and transcriptional control of Fas ligand gene expression. Cell Death Differ 2003;10:36–44.
[38] Wajant H. The Fas signaling pathway: more than a paradigm. Science 2002;296:1635–6.
[39] Kuwana T, Smith JJ, Muzio M, Dixit V, Newmeyer DD, Kornbluth S. Apoptosis induction by caspase-8 is amplified through the mitochondrial release of cytochrome c. J Biol Chem 1998;273:16589–94.
[40] De Groote D, Zangerle PF, Gevaert Y, Fassotte MF, Beguin Y, Noizat-Pirenne F, et al. Direct stimulation of cytokines (IL-1β, TNF-β, IL-6, IL-2, IFN-γ and GM-CSF) in whole blood. I. Comparison with isolated PBMC stimulation. Cytokine 1992;4:239–48.
[41] Feghali CA, Wright TM. Cytokines in acute and chronic inflammation. Front Biosci 1997;2:d12–26.
[42] Makovitzki A, Fink A, Shai Y. Suppresion of human solid tumor growth in mice by intratumor and systemic inocation of histidine-rich and pH-dependent host defense-lie lytic peptides. Cancer Res 2009;69:3458–63.